



Control of hot-carrier relaxation time in Au-Ag thin films through alloying

SARVENAZ MEMARZADEH,^{1,2}  KEVIN J. PALM,^{2,3} THOMAS E. MURPHY,^{1,2}  MARINA S. LEITE,⁴ AND JEREMY N. MUNDAY^{1,5,*}

¹Department of Electrical and Computer Engineering, University of Maryland, College Park, Maryland 20742, USA

²Institute for Research in Electronics and Applied Physics, University of Maryland, College Park, Maryland 20742, USA

³Department of Physics, University of Maryland, College Park, Maryland 20742, USA

⁴Department of Materials Science and Engineering, University of California, Davis, CA 95616, USA

⁵Department of Electrical and Computer Engineering, University of California, Davis, CA 95616, USA

*jnmunday@ucdavis.edu

Abstract: The plasmon resonance of a structure is primarily dictated by its optical properties and geometry, which can be modified to enable hot-carrier photodetectors with superior performance. Recently, metal alloys have played a prominent role in tuning the resonance of plasmonic structures through chemical composition engineering. However, it has been unclear how alloying modifies the time dynamics of the generated hot-carriers. In this work, we elucidate the role of chemical composition on the relaxation time of hot-carriers for the archetypal $\text{Au}_x\text{Ag}_{1-x}$ thin film system. Through time-resolved optical spectroscopy measurements in the visible wavelength range, we measure composition-dependent relaxation times that vary up to 8× for constant pump fluency. Surprisingly, we find that the addition of 2% of Ag into Au films can increase the hot-carrier lifetime by approximately 35% under fixed fluence, as a result of a decrease in optical loss. Further, the relaxation time is found to be inversely proportional to the imaginary part of the permittivity. Our results indicate that alloying is a promising approach to effectively control hot-carrier relaxation time in metals.

© 2020 Optical Society of America under the terms of the [OSA Open Access Publishing Agreement](#)

1. Introduction

Pure metals, such as gold (Au) and silver (Ag), have long been the most commonly used plasmonic materials due to their high electron densities and desirable optical and chemical properties [1–7]. However, when using pure metals, applications are limited to a narrow range of optical frequencies stemming from the inherent resonances of the metals. Alloying these metals together presents a promising alternative by allowing the opportunity to tune the plasmonic resonances without altering the geometry of the system. The optical properties of the Au-Ag alloys can be tailored throughout the visible spectrum by modifying the atomic ratio of the two metals [8–11].

Additionally, by varying the alloy's chemical composition, one can modify the electronic band structure, which results in interband transitions over different incident photon energies. It was recently reported that as the concentration of Au increases in Au-Ag alloyed films, the position of the d-band shifts closer to the Fermi level [12]. This reduces the energy gap for interband transitions, leading to transitions occurring with lower incident photon energies. Similar modification of the threshold of the interband transitions has also been studied in other types of materials such as metal nitrides [13], semiconductors [14], and transition metal dichalcogenides [15]. The resonance tunability and band structure engineering of alloys proves useful in a variety of applications including superabsorbers [16], imaging probes in biomolecular studies [17,18], implant devices [19], catalysis [20–22], photovoltaics [23,24], and hydrogen sensing [25–28].

Many of the aforementioned applications rely on significant light absorption within the films or nanostructures. One common approach for absorption enhancement is through coupling the incident photons into surface plasmons, i.e. coherent oscillations of free electrons at the metal-dielectric interface. This process results in the generation of highly energetic non-thermal carriers, also known as hot-carriers. Particularly, hot-carriers are generated after nonradiative decay of the localized or propagating surface plasmons through either direct or phonon-assisted intraband transitions [29,30]. Once these carriers are excited, they thermalize to create a population of electrons that can be described as a Fermi-Dirac distribution at an elevated temperature. They start to equilibrate with the lattice temperature via a series of scattering processes including the electron-phonon and phonon-phonon scatterings [31,32]. These highly energetic carriers have been utilized in applications such as water splitting [33], artificial photosynthesis [34], medical therapy [35], and drug delivery [36]. However, efficient generation and extraction of these carriers depends on the choice of material, and their corresponding hot-carrier relaxation time. In particular, understanding of the hot-carrier relaxation time plays a significant role in modulation speed [37], power conversion efficiency enhancement [38,39], determining the hot-electron flux [40,41], and nanoscale photothermal heat control [42]. Thus, due to the broad spectral tunability associated with devices exploiting hot-carrier physics, their temporal study in planar Au-Ag structures would benefit a variety of applications.

Here, we focus on Au-based hot-carrier devices due to their chemical stability and incorporate different ratios of Ag to create Au-Ag alloys. We use ultrafast pump-probe optical spectroscopy to measure the hot-carrier relaxation time. The pump wavelength is nominally set to 700 nm wavelength (1.77 eV) to ensure that the relaxation time is due to intraband transitions rather than interband ones (2.4 eV in Au and 4.0 eV in Ag) [12,43]. We further employ the Kretschmann geometry to couple into the propagating surface plasmon mode, which has the added benefit of increasing the measurement sensitivity as a result of increased photon absorption. To determine the hot-carrier lifetime, we use a free-electron model and convert the differential reflectivity measurements to the corresponding elevated electron temperature [44]. Our results show that the hot-carrier relaxation time depends upon the Ag mole fractions. We further find that the lifetime is inversely proportional to the imaginary part of the permittivity for different Au-Ag alloys. Finally, considering the pure Au film as the baseline of the lifetime measurements, we observe that the slight addition of Ag (2%) can increase the hot-carrier relaxation time, while higher fractions of Ag (e.g. 35% and 75%) yield smaller lifetimes.

2. Results and discussion

To study the effect of alloying on the hot-carrier relaxation time, we fabricated four samples with different Au-Ag compositions using a co-sputtering deposition procedure. The thickness of samples are 35 nm, 42 nm, 25 nm, and 21 nm for different Au-Ag alloys from low to high Ag concentration, respectively. We change the alloys composition by varying the applied voltage on the Au and Ag targets during each deposition, which results in the formation of thin films of $\text{Au}_x\text{Ag}_{100-x}$ with $x = 100, 98, 65, \text{ and } 25$. The chemical composition of the alloyed samples is determined with energy-dispersive X-ray spectroscopy (EDX) (Fig. 1(a)). Figures 1(b) and 1(c) show the AFM topography and roughness distribution of Au-Ag alloys. Subsequently, we measure the optical properties of our samples with spectroscopic ellipsometry in the wavelength range from 200 nm to 1000 nm. We use a Drude-Lorentz model including two Drude and one Lorentz terms to fit the ellipsometry data. The modelled permittivity is shown in Figs. 2(a) and 2(b) for our fabricated samples. We also compute the surface plasmon polariton (SPP) quality factor, $Q_{spp}(\omega) = \epsilon_r^2(\omega)/\epsilon_i(\omega)$ [45], for the different Au-Ag alloys (Fig. 2(c)). In general, many experimental factors such as the chamber pressure, substrate temperature, deposition rate, etc. can affect the films' quality factors due to the change in the dielectric functions [46]. Our experiments keep all of these other factors the same, thus isolating the effects of changing the

alloy composition. At 700 nm, the wavelength used for our pump-probe measurements, the 100% Au and 98% Au samples show a higher Q_{spp} when compared to the other alloys, predominantly due to the lower ϵ_i . The dielectric functions can also be affected by a disordered mixture of Au and Ag at a certain molar combination, leading to the reduction of electron scattering and plasma frequency [12,47]. Additionally, it has been shown that the co-sputtering of a small amount of metal suppresses the island growth, leading to a film with low optical and electrical losses [23]. Furthermore, it has also been shown that the imaginary part of the dielectric function of a thin film, which is responsible for the optical losses, generally increases with the decrease of the film thickness for gold films below 80 nm [48]. We have compared the optical properties of our pure gold sample with that of a pure gold film obtained from [48] (gray lines in Fig. 2), showing good agreement. We further hypothesize that by varying the thickness of the different AuAg alloys,

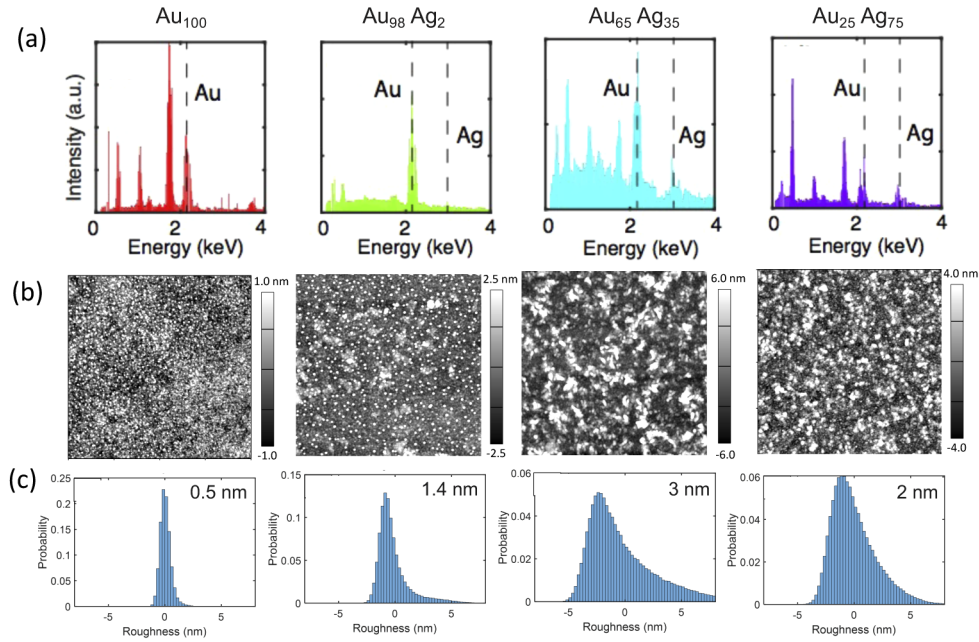


Fig. 1. Chemical and structural properties of thin films. (a) EDX. (b) AFM topography. (c) Roughness distribution. Insets show RMS roughnesses.

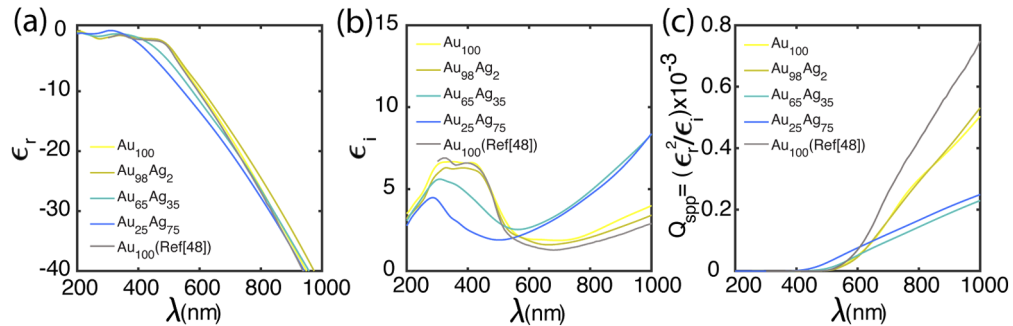


Fig. 2. Optical response of Au_x Ag_{1-x} alloys. Measured (a) real and (b) imaginary parts of the permittivity, and (c) computed quality factor of the propagating surface plasmon.

the relaxation time of the excited hot-carriers could be further tuned due to the variation in the optical losses in these films.

Before measuring the relaxation dynamics of the excited hot-carriers, we measured the propagating surface plasmon mode using the Kretschmann configuration [49]. Figure 3(a) shows the experimental results of the reflection measurements for all four samples as a function of incident angle near the plasmon coupling angle for incident wavelength from 680 nm to 740 nm with 5 nm spectral bandwidth.

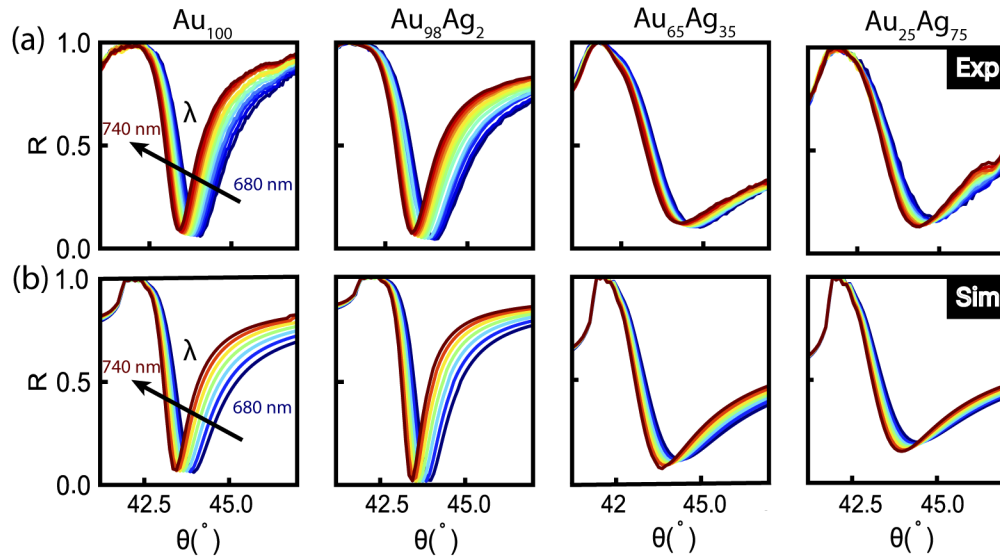


Fig. 3. (a) Experimental and (b) simulated reflectivity for Au, Au₉₈Ag₂, Au₆₅Ag₃₅, and Au₂₅Ag₇₅ alloys under p-polarized illumination with wavelengths ranging from 680 nm to 740 nm. For FDTD simulations, we used pulse illumination with 150 fs pulse width.

We utilized the Finite Difference Time Domain (FDTD) method (Lumerical Inc.) for the reflection calculations (Fig. 3(b)). The optical properties of the samples are extracted from the ellipsometry measurements and used as inputs for the simulations. A perfectly match layer (PML) boundary condition with 64 layers is used for the boundaries along with a non-uniform mesh setting with an accuracy of 4. Similar to our experimental conditions, the incident source has a pulse width of 150 fs. The incident angle is swept from 40 to 48 degrees with 0.1-degree increments for each wavelength between 680 nm and 740 nm. There is a good agreement between the FDTD simulation results and the experimental measurements. As expected, the surface plasmon resonance is sharper for samples with higher Q_{spp} and broader for the samples with lower values.

The non-equilibrium hot-carrier dynamics of the alloys are investigated using degenerate ($\lambda_{pump} = \lambda_{probe}$) time-resolved differential reflectivity measurements at the surface plasmon resonance angle. We use a Ti-Sapphire laser system with 700 nm wavelength and 80 MHz repetition rate to generate both the pump and probe beams. A fraction of the laser beam is split off to serve as the probe beam and the other portion is passed through a mechanical delay stage to set the time delay between the two beams. We use nearly co-linear pump and probe beams, which are adjusted to couple into the propagating surface plasmon mode but can also be spatially separated in the reflected field. The overlap of the beams is achieved using an off-axis parabolic mirror with a measured spot size of approximately 90 μm . Pump-probe measurements are conducted at the surface plasmon resonance angle under five different incident pump powers

(i.e. 120 mW, 150 mW, 180 mW, 210 mW, and 240 mW) with a fixed probe power of 19.8 mW, as shown in Fig. 4.

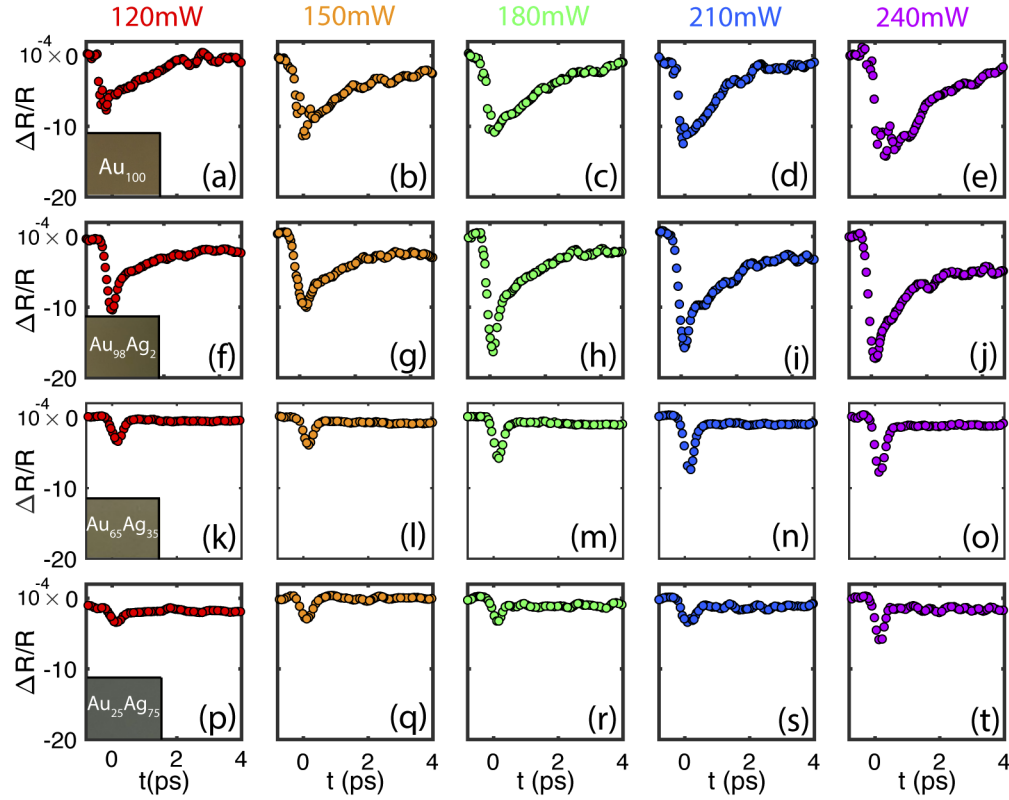


Fig. 4. Differential reflectivity measurements for Au-Ag alloys with different chemical compositions. For each sample, the pump power is: 120 mW (a,f,k,p), 150 mW (b,g,l,q), 180 mW (c,h,m,r), 210 mW (d,i,n,s), and 240 mW (e,j,o,t). Insets are real-color photographs of the alloyed thin films.

As expected, in all cases, increasing the pump power produces a larger change in the transient reflectivity ($\Delta R/R$). Because the temporal pulse width employed here is longer than the electron-electron scattering time, on the order of 100 fs [50], the relaxation time for the optically excited hot-carriers is mostly governed by the electron-phonon relaxation time. Furthermore, at the resonance wavelength, the pump-induced change in the reflectivity signal is negative, which is attributed to the intraband transition and the excitation of hot-carriers for the fabricated alloys [50,51]. It is also worth mentioning that both hot-electrons and hot-holes can contribute to device performance, see for example the use of hot-holes for photochemical reactions [52]. Gong et al. showed how the energy of the hot-carrier distribution depends not only on the Electron Density of States (EDS) but also on the energy of the incident photons and how it can be modified for a variety of structures [53]. For the 700 nm wavelength illumination used in our study, hot-hole extraction is more efficient than the hot-electrons extraction in pure Au, as the distribution of hot-holes is peaked further away from the Fermi level. However, for the case of the Au-Ag mixtures, the distributions of both hot-holes and hot-electrons become more uniform as the illumination wavelength approaches the Near-IR range [54]; thus, both of these excited hot-carriers will have similar contributions to the overall hot-carrier effects. We also note that the differences between the hot-hole and hot-electron distributions in Au and Au-Ag

alloys can provide additional tunability for the carrier extraction depending upon the materials and functionality of the rest of the device. Further, the threshold for the interband transition for Au-Ag alloys shifts to a longer wavelengths as the Au content increases, allowing for additional control of these processes [12,54].

3. Theory and analysis

To find the excited hot-carrier relaxation time from the transient reflectivity measurements, we employ the combination of a free-electron model [55] and the modified two-temperature model [44]. In this model, the effect of the surface plasmon's electric field profile is incorporated into the absorbed laser power density within the conventional two-temperature model, which accounts for variation of the field in the vertical (surface normal) direction. This combination allows us to convert the pump-probe reflectivity signal to the relevant electron temperature, which results in more accurate theoretical modeling due to the nonlinear relationship between the reflectivity signal and the electron temperature. The model uses the optical parameters extracted from our ellipsometry measurements at room temperature for each alloy. Finally, best fits to the temperature converted reflectivity signals are computed by minimizing the Normalized Mean Squared Error (NMSE) of the hot-carrier relaxation time. Figure 5 shows the results of the temperature converted data (filled circles) and their corresponding best fits (solid lines) to the hot-carrier relaxation time of the alloyed Au-Ag films at pump powers of 120, 150, 180, 210, and 240 mW under the resonance condition, i.e. upon coupling to the surface plasmon mode.

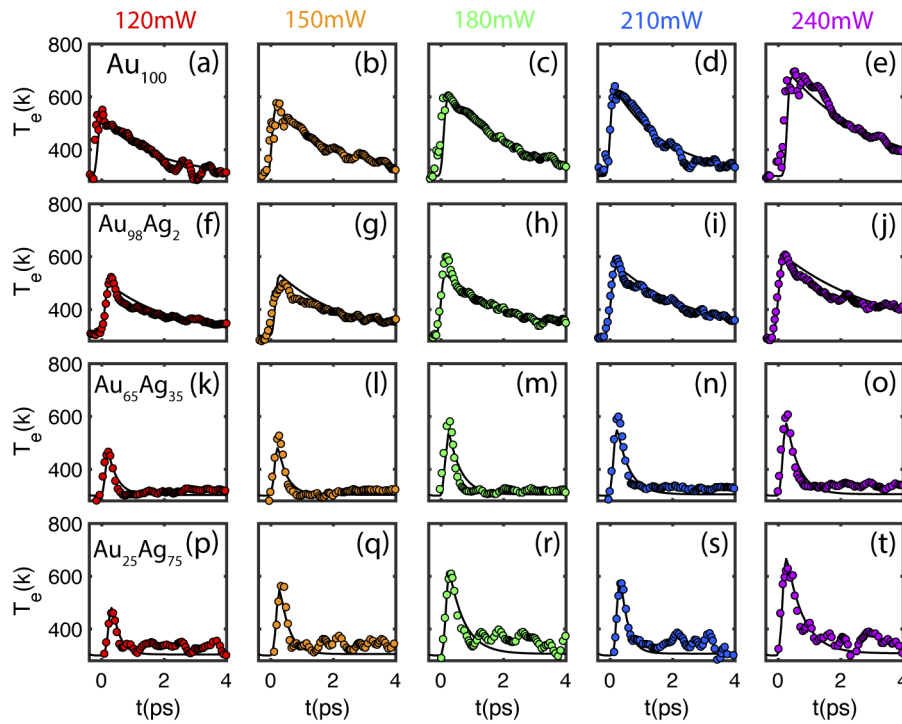


Fig. 5. Temperature converted differential reflectivity measurements for Au_{100} , $\text{Au}_{98}\text{Ag}_2$, $\text{Au}_{65}\text{Ag}_{35}$, and $\text{Au}_{25}\text{Ag}_{75}$ alloys under different incident pump powers of 120 mW (a,f,k,p), 150 mW (b,g,l,q), 180 mW (c,h,m,r), 210 mW (d,i,n,s), and 240 mW (e,j,o,t). The black solid lines in each plot show the best fits computed from a modified two-temperature model.

The pump-probe measurements also reveal an additional short decay component that only appears immediately after excitation for the 2% Ag composition. We attribute this decay component to electron-electron interactions, which are typically too fast to be detected in the pure Au. The plasmon dephasing time (i.e. the rate at which electron's collective oscillations cease) is longer in Ag as a result of different radiative or non-radiative plasmon damping mechanisms, and so the addition of Ag to the Au alloy may increase this decay component to a measurable amount in the 2% Ag alloy. For the higher Ag concentration alloys, this decay mechanism is not distinguishable from electron-phonon interactions based on our measurement sensitivity.

Analysis of the temperature converted differential reflectivity shows that the hot-carrier relaxation time (τ) of the $\text{Au}_{98}\text{Ag}_2$ sample is ~ 8 times larger than for $\text{Au}_{65}\text{Ag}_{35}$ and $\text{Au}_{25}\text{Ag}_{75}$ for a fixed laser fluence. Additionally, we find that the film with $\text{Au}_{98}\text{Ag}_2$ has the longest lifetime of any of the samples measured (3.20 ± 0.15 ps with 240 mW pump power), even including pure Au. To further investigate this phenomenon, we consider the optical properties of each Au-Ag alloy at 700 nm pump wavelength and compare the result with our measured hot-carrier relaxation time, and find τ to be inversely proportional to the imaginary part of the permittivity (Fig. 6).

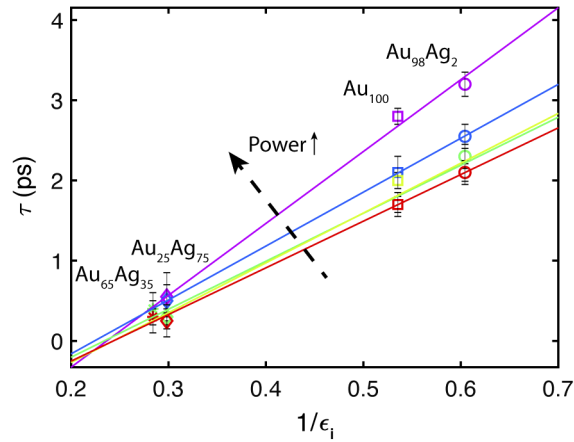


Fig. 6. Hot-carrier relaxation time as a function of $1/\epsilon_i$, the inverse of the imaginary part of the permittivity, for $\text{Au}_x\text{Ag}_{1-x}$. The solid lines are the linear fit between the hot-carrier lifetime and $1/\epsilon_i$. The colors represent the range of the pump power between 120 mW (red) to 240 mW (purple).

Our results suggest that the addition of a small fraction (2%) of Ag to a Au film increases the hot-carrier lifetime. This is consistent with previous findings that showed particular Ag-Au alloys having higher Q_{spp} than pure metals [11] and that doping one metal with another can improve film quality and decrease optical loss [23,56]. However, all alloyed films that we measured have similar surface roughnesses, suggesting that the decreased loss may come from changes in the band structure or other changes to the material rather than simply smoothing of the films. Because we are probing relaxation times > 10 s of fs, the main mechanism leading to the increase in the hot-carrier lifetime is likely a suppression of the electron-phonon scattering, which could result for decreased lattice defects, grain boundaries, etc., but further work will be necessary to isolate the individual contributions. In addition, the lifetime is inversely proportional to ϵ_i and increases with pump power (see Fig. 6 for a comparison with all pump powers), which is in agreement with previously reported studies [57,58]. These results show that the optical loss is an important and potentially controllable internal parameter compared to the other external factors, such as pump power. Our observation further opens a new route to alter the hot-carrier relaxation time for plasmonic applications through alloying. In the future, photoluminescence

(PL) spectroscopy of the AuAg alloys could enable a better understanding of the contribution of the intraband transitions to light emission for the individual alloys [59,60].

4. Conclusion

In summary, we measured the hot-carrier relaxation time of Au-Ag thin film alloys under visible excitation and found that adding a small fraction of Ag to Au increases the hot-carrier relaxation time. Our experimental results suggested that the relaxation time depends on the alloy's composition and is inversely proportional to ϵ_i . Surprisingly, some alloys can have loss factors that are less than their pure counterparts, which leads to improved hot-carrier performance. By comparing the relaxation time of the fabricated alloys with the pure Au sample, we determined that the measured relaxation time increases with slight addition of Ag and then drops significantly for alloys with higher Ag content. Overall, this work demonstrated that the relaxation time of hot-carriers can be engineered through alloying.

Funding

National Science Foundation (CAREER ECCS-1554503, MMN-2016617, MMN-1609414); Office of Naval Research YIP (N00014-16-1-2540).

Acknowledgments

SM acknowledges financial support from a Graduate School Summer Research Fellowship and support from the FabLab at the University of Maryland Nanocenter. KJP acknowledges financial support from a National Defense Science and Engineering Graduate Fellowship.

Disclosures

The authors declare no conflicts of interest.

References

1. S. A. Maier, *Plasmonics: Fundamentals and Applications* (Springer, 2018).
2. S. J. Oldenburg, R. D. Averitt, S. L. Westcott, and N. J. Halas, "Nanoengineering of optical resonances," *Chem. Phys. Lett.* **288**(2-4), 243–247 (1998).
3. S. A. Maier, M. L. Brongersma, P. G. Kik, S. Meltzer, A. A. Requicha, and H. A. Atwater, "Plasmonics - A route to nanoscale optical devices," *Adv. Mater.* **13**(19), 1501–1505 (2001).
4. V. E. Ferry, J. N. Munday, and H. A. Atwater, "Design considerations for plasmonic photovoltaics," *Adv. Mater.* **22**(43), 4794–4808 (2010).
5. X. Z. Nicholas Fang, H. Lee, and C. Sun, "Sub-Diffraction-Limited Optical Imaging with a Silver Superlens," *Science* **308**(5721), 534–537 (2005).
6. V. M. Shalaev, W. Cai, U. Chettiar, H. K. Yuan, A. K. Sarychev, V. P. Drachev, and A. V. Kildishev, "Negative index of refraction in optical metamaterials," *Opt. Lett.* **30**(24), 3356–3358 (2005).
7. D. O. S. Melville and R. J. Blaikie, "Super-resolution imaging through a planar silver layer," *Opt. Express* **13**(6), 2127 (2005).
8. S. Kadkhodazadeh, F. A. A. Nugroho, C. Langhammer, M. Beleggia, and J. B. Wagner, "Optical Property-Composition Correlation in Noble Metal Alloy Nanoparticles Studied with EELS," *ACS Photonics* **6**(3), 779–786 (2019).
9. Y. Bai, C. Gao, and Y. Yin, "Fully alloyed Ag/Au nanorods with tunable surface plasmon resonance and high chemical stability," *Nanoscale* **9**(39), 14875–14880 (2017).
10. X. Wang, G. Ma, A. Li, J. Yu, Z. Yang, J. Lin, A. Li, X. Han, and L. Guo, "Composition-adjustable Ag-Au substitutional alloy microcages enabling tunable plasmon resonance for ultrasensitive SERS," *Chem. Sci.* **9**(16), 4009–4015 (2018).
11. C. Gong and M. S. Leite, "Noble Metal Alloys for Plasmonics," *ACS Photonics* **3**(4), 507–513 (2016).
12. C. Gong, A. Kaplan, Z. A. Benson, D. R. Baker, J. P. McClure, A. R. Rocha, and M. S. Leite, "Band Structure Engineering by Alloying for Photonics," *Adv. Opt. Mater.* **6**(17), 1800218 (2018).
13. M. Kumar, S. Ishii, N. Umezawa, and T. Nagao, "Band engineering of ternary metal nitride system Ti_{1-x}Zr_xN for plasmonic applications," *Opt. Mater. Express* **6**(1), 29 (2016).
14. C. Z. N. Peidong Yang, L. Dou, and P. Yang, "Bandgap engineering in semiconductor alloy nanomaterials with widely tunable compositions," *Nat. Rev. Mater.* **2**, 1–15 (2017).

15. T. Gong and J. N. Munday, "Angle-Independent Hot Carrier Generation and Collection Using Transparent Conducting Oxides," *Nano Lett.* **15**(1), 147–152 (2015).
16. M. R. S. Dias, C. Gong, Z. A. Benson, and M. S. Leite, "Lithography-Free, Omnidirectional, CMOS-Compatible AlCu Alloys for Thin-Film Superabsorbers," *Adv. Opt. Mater.* **6**(2), 1700830 (2018).
17. J. Ando, A. Nakamura, M. Yamamoto, C. Song, K. Murata, and R. Iino, "Multicolor High-Speed Tracking of Single Biomolecules with Silver, Gold, and Silver-Gold Alloy Nanoparticles," *ACS Photonics* **6**(11), 2870–2883 (2019).
18. G. Azarfar, E. Aboulizadeh, N. M. Walter, S. Ratti, C. Olivieri, A. Norici, M. Nasse, A. Kohler, M. Giordano, and C. J. Hirschmugl, "Estimating and correcting interference fringes in infrared spectra in infrared hyperspectral imaging," *Analyst* **143**(19), 4674–4683 (2018).
19. M. Niinomi, M. Nakai, and J. Hieda, "Development of new metallic alloys for biomedical applications," *Acta Biomater.* **8**(11), 3888–3903 (2012).
20. X. Liu, D. Wang, and Y. Li, "Synthesis and catalytic properties of bimetallic nanomaterials with various architectures," *Nano Today* **7**(5), 448–466 (2012).
21. D. Wang and Y. Li, "Bimetallic Nanocrystals: Liquid-Phase Synthesis and Catalytic Applications," *Adv. Mater.* **23**(9), 1044–1060 (2011).
22. P. Hernández-Fernández, S. Rojas, P. Ocón, J. L. De La Fuente, J. S. Fabián, J. Sanza, M. A. Peña, F. J. García-García, P. Terreros, and J. L. Fierro, "Influence of the preparation route of bimetallic Pt-Au nanoparticle electrocatalysts for the oxygen reduction reaction," *J. Phys. Chem. C* **111**(7), 2913–2923 (2007).
23. C. Zhang, D. Zhao, D. Gu, H. Kim, T. Ling, Y. K. R. Wu, and L. J. Guo, "An ultrathin, smooth, and low-loss Al-doped Ag film and its application as a transparent electrode in organic photovoltaics," *Adv. Mater.* **26**(32), 5696–5701 (2014).
24. E. Kheirandish, J. C. Marnocha, and N. Kouklin, "Controlling opto-electronic characteristics of ternary II-VI alloyed quantum dots: alcohol processing assay," *Mater. Res. Express* **7**(7), 075008 (2020).
25. C. Wadell, F. Anggoro Ardy Nugroho, E. Lidstro, B. Iandolo, J. B. Wagner, and C. Langhammer, "Hysteresis-Free Nanoplasmonic Pd-Au Alloy Hydrogen Sensors," *Nano Lett.* **15**(5), 3563–3570 (2015).
26. F. A. Nugroho, I. Darmadi, L. Cusinato, A. Susarrey-Arce, H. Schreuders, L. J. Bannenberg, A. B. da Silva Fanta, S. Kadkhodazadeh, J. B. Wagner, T. J. Antosiewicz, A. Hellman, V. P. Zhdanov, B. Dam, and C. Langhammer, "Metal–polymer hybrid nanomaterials for plasmonic ultrafast hydrogen detection," *Nat. Mater.* **18**(5), 489–495 (2019).
27. K. J. Palm, J. B. Murray, J. P. McClure, M. S. Leite, and J. N. Munday, "In Situ Optical and Stress Characterization of Alloyed $\text{Pd}_x\text{Au}_{1-x}$ Hydrides," *ACS Appl. Mater. Interfaces* **11**(48), 45057–45067 (2019).
28. Y. Nishijima, S. Shimizu, K. Kurihara, Y. Hashimoto, H. Takahashi, A. Balcytis, G. Seniutinas, S. Okazaki, J. Juodkazyt, T. Iwasa, T. Taketsugu, Y. Tominaga, S. Juodkazyt, S. K. Earl, T. D. James, T. J. Davis, J. C. McCallum, R. E. Marvel, R. F. Haglund, and A. Roberts, "Optical readout of hydrogen storage in films of Au and Pd," *Opt. Express* **25**(20), 24081–24092 (2017).
29. R. Sundararaman, P. Narang, A. S. Jermyn, W. A. Goddard III, and H. A. Atwater, "Theoretical predictions for hot-carrier generation from surface plasmon decay," *Nat. Commun.* **5**(1), 5788 (2014).
30. A. M. Brown, R. Sundararaman, P. Narang, W. A. G. Iii, H. A. Atwater, and T. J. Watson, "Nonradiative Plasmon Decay and Hot Carrier Dynamics: Effects of Phonons, Surfaces, and Geometry," *ACS Nano* **10**(1), 957–966 (2016).
31. J. H. Hodak, A. Henglein, and G. V. Hartland, "Photophysics of Nanometer Sized Metal Particles: Electron-Phonon Coupling and Coherent Excitation of Breathing Vibrational Modes," *J. Phys. Chem. B* **104**(43), 9954–9965 (2000).
32. C. Voisin, N. D. Fatti, D. Christofilos, and F. Vallée, "Ultrafast Electron Dynamics and Optical Nonlinearities in Metal Nanoparticles," *J. Phys. Chem. B* **105**(12), 2264–2280 (2001).
33. A. Naldoni, F. Riboni, U. Guler, A. Boltasseva, V. M. Shalaev, and A. V. Kildishev, "Solar-Powered Plasmon-Enhanced Heterogeneous Catalysis," *Nanophotonics* **5**(1), 112–133 (2016).
34. S. Mubeen, J. Lee, N. Singh, S. Krämer, G. D. Stucky, and M. Moskovits, "An autonomous photosynthetic device in which all charge carriers derive from surface plasmons," *Nat. Nanotechnol.* **8**(4), 247–251 (2013).
35. P. K. Jain, I. H. ElSayed, and M. A. El-Sayed, "Au nanoparticles target cancer," *Nano Today* **2**(1), 18–29 (2007).
36. G. Han, P. Ghosh, and M. M. De Vincent Rotello, "Drug and Gene Delivery using Gold Nanoparticles," *Nanobiotechnol.* **3**(1), 40–45 (2007).
37. O. L. Muskens, L. Bergamini, Y. Wang, J. M. Gaskell, N. Zabala, C. H. De Groot, D. W. Sheel, and J. Aizpurua, "Antenna-assisted picosecond control of nanoscale phase transition in vanadium dioxide," *Light: Sci. Appl.* **5**(10), e16173 (2016).
38. F. Wang and N. A. Melosh, "Plasmonic Energy Collection through Hot Carrier Extraction," *Nano Lett.* **11**(12), 5426–5430 (2011).
39. W. Li and J. Valentine, "Metamaterial Perfect Absorber Based Hot Electron Photodetection," *Nano Lett.* **14**(6), 3510–3514 (2014).
40. A. Pandey and P. Guyot-Sionnest, "Slow Electron Cooling in Colloidal," *Science* **322**(5903), 929–932 (2008).
41. G. J. Conibeer, D. König, M. A. Green, and J. F. Guillemoles, "Slowing of carrier cooling in hot carrier solar cells," *Thin Solid Films* **516**(20), 6948–6953 (2008).
42. Z. J. Coppens, W. Li, D. G. Walker, and J. G. Valentine, "Probing and Controlling Photothermal Heat Generation in Plasmonic Nanostructures," *Nano Lett.* **13**(3), 1023–1028 (2013).

43. D. Rioux, S. Vallières, S. Besner, P. Mu noz, E. Mazur, and M. Meunier, "An analytic model for the dielectric function of Au, Ag, and their Alloys," *Adv. Opt. Mater.* **2**(2), 176–182 (2014).
44. S. Memarzadeh, J. Kim, Y. Aytac, T. Murphy, and J. Munday, "Surface Plasmon Assisted Control of Hot-Electron Relaxation Time," *Optica* **7**(6), 608–612 (2020).
45. P. R. West, S. Ishii, G. V. Naik, N. K. Emani, V. M. Shalae, and A. Boltasseva, "Searching for better plasmonic materials," *Laser Photonics Rev.* **4**(6), 795–808 (2010).
46. K. M. Mcpeak, S. V. Jayanti, S. J. P. Kress, S. Meyer, S. Iotti, A. Rossinelli, and D. J. Norris, "Plasmonic Films Can Easily Be Better: Rules and Recipes," *ACS Photonics* **2**(3), 326–333 (2015).
47. Y. Nishijima and S. Akiyama, "Unusual optical properties of the Au/Ag alloy at the matching mole fraction," *Opt. Mater. Express* **2**(9), 1226–1235 (2012).
48. D. I. Yakubovsky, A. V. Arsenin, Y. V. Stebunov, D. Y. Fedyanin, and V. S. Volkov, "Optical constants and structural properties of thin gold films," *Opt. Express* **25**(21), 25574 (2017).
49. O. Pluchery, R. Vayron, and K.-M. Van, "Laboratory experiments for exploring the surface plasmon resonance," *Eur. J. Phys.* **32**(2), 585–599 (2011).
50. C. K. Sun, F. Vallée, L. H. Acioli, E. P. Ippen, and J. G. Fujimoto, "Femtosecond-tunable measurement of electron thermalization in gold," *Phys. Rev. B* **50**(20), 15337–15348 (1994).
51. Y. Aytac, M. Mittendorf, and T. E. Murphy, "Probing the free-carrier absorption in multi-layer black phosphorus," *Appl. Phys. Lett.* **113**(3), 031108 (2018).
52. E. Pensa, J. Gargiulo, A. Lauri, S. Schlücker, E. Cortés, and S. A. Maier, "Spectral Screening of the Energy of Hot Holes over a Particle Plasmon Resonance," *Nano Lett.* **19**(3), 1867–1874 (2019).
53. T. Gong and J. N. Munday, "Materials for hot carrier plasmonics," *Opt. Mater. Express* **5**(11), 2501–2512 (2015).
54. L. J. Kray, K. J. Palm, C. Gong, A. Torres, C. E. Villegas, A. R. Rocha, M. S. Leite, and J. N. Munday, "Enhanced near-Infrared Photoresponse from Nanoscale Ag-Au Alloyed Films," *ACS Photonics* **7**(7), 1689–1698 (2020).
55. P. Guo, R. D. Schaller, J. B. Ketterson, and R. P. H. Chang, "Ultrafast switching of tunable infrared plasmons in indium tin oxide nanorod arrays with large absolute amplitude," *Nat. Photonics* **10**(4), 267–273 (2016).
56. D. Gu, C. Zhang, Y. K. Wu, and L. J. Guo, "Ultrasmooth and thermally stable silver-based thin films with subnanometer roughness by aluminum doping," *ACS Nano* **8**(10), 10343–10351 (2014).
57. J. Hodak, I. Martini, and G. V. Hartland, "Ultrafast study of electron-phonon coupling in colloidal gold particles," *Chem. Phys. Lett.* **284**(1-2), 135–141 (1998).
58. M. M. Alvarez, J. T. Khoury, T. G. Schaaff, M. N. Shafigullin, I. Vezmar, and R. L. Whetten, "Optical Absorption Spectra of Nanocrystal Gold Molecules," *J. Phys. Chem. B* **101**(19), 3706–3712 (1997).
59. Y. Y. Cai, J. G. Liu, L. J. Tauzin, D. Huang, E. Sung, H. Zhang, A. Joplin, W. S. Chang, P. Nordlander, and S. Link, "Photoluminescence of Gold Nanorods: Purcell Effect Enhanced Emission from Hot Carriers," *ACS Nano* **12**(2), 976–985 (2018).
60. B. Ostovar, Y.-Y. Cai, L. J. Tauzin, S. A. Lee, A. Ahmadi, R. Zhang, P. Nordlander, and S. Link, "Increased intraband transitions in smaller gold nanorods enhance light emission," *ACS Nano* **0**, null (0). PMID: 32852941.